Journal of Statistical Physics, Vol. 68, Nos. 5/6, 1992

Modulated Phases and Upsilon Points in a Spin Model with Helical Ordering

Kazuo Sasaki[1]

Received November 8, 1991; final February 25, 1992

The ground state of a one-dimensional, classical XY model with competing nearest- and next-nearest-neighbor interactions, a sixfold anisotropy, and an external field is studied. The model shows various modulated phases, depending on the values of the model parameters. Evidence is found that the ground-state phase diagram of this model contains *upsilon points*, multicritical points of a new class recently discussed by Bassler, Sasaki, and Griffiths. The phase diagram has a self-similar structure near these points, filled with multitudes of "mixed phases" whose spin configurations consist of segments of helical and fan structures separated by interfaces between them.

KEY WORDS: Modulated phases; XY model; ground states; helical spin structures; interfaces; interface interactions; phase diagrams.

1. INTRODUCTION

Phase transitions in systems which have a spatially modulated structure, the period of which may be commensurate or incommensurate with that of an underlying lattice, have attracted much theoretical attention; see review articles[1–5] and references therein. It is often the case that a complex modulated structure can be thought of as consisting of domains of a simple commensurate structure separated by defects (domain walls, discommensurations, solitons, etc.). In certain situations, the nature of transition from one modulated phase to another can be understood in terms of defect interactions. For example, Villain and Gordon[6] studied defect interactions to investigate the phase diagram near the multiphase point[7] in the axial next-nearest-neighbor Ising (ANNNI) model. More recently, Fisher and

[1] Department of Engineering Science, Faculty of Engineering, Tohoku University, Sendai 980, Japan.

0022-4715/92/0900-1013$06.50/0

Szpilka[8–11] carefully defined *multi*defect interactions to analyze systematically phase diagrams of systems which have uniaxially modulated structures, and found interesting phenomena such as a *quasitricritical point.* Their analysis was extended by Bassler *et al.*[12] to the case in which modulated structures can be described as consisting of domains of two distinct types separated by interfaces rather than as consisting of domains of a single type separated by defects (the two pictures are equivalent if a defect is a bound pair of interfaces). The extended analysis revealed certain new features which can appear in phase diagrams. The present paper deals with one such feature: an *upsilon point.*

An upsilon point is an endpoint of a first-order transition line from which infinitely many phases "spring out." Figure 1 schematically shows a phase diagram, in some parameter space, in the vicinity of an upsilon point which is the left endpoint of the transition line between phases α and β. Here the dashed lines are first-order lines and the solid lines represent collections of (infinitely many) transition lines which are bunched together so tightly that individual lines are not visible. The unlabeled, fan-shaped region is filled with multitudes of "mixed phases," each of which has a superlattice structure consisting of alternating domains of phases α and β separated by parallel interfaces. The sides of the fan together with the first-order line between phases α and β form a shape resembling the Greek letter Υ lying on its side—hence the name upsilon point. (In this respect an upsilon point is analogous to a bicritical point at which two critical lines

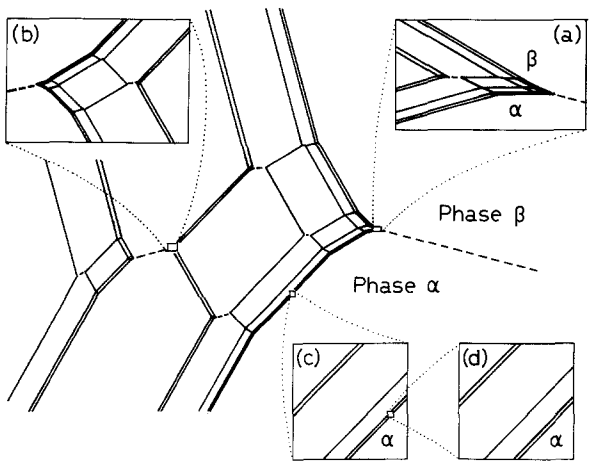

Fig. 1. Schematic phase diagram, in some parameter space, in the vicinity of an upsilon point at the left end of the transition line between phases α and β. The dashed lines are first-order transitions and the solid lines represent collections of infinitely many transition lines. The magnifications of various portions of the phase diagram are shown as the insets (a)–(d).

merge to form a first-order line, but quite different in other respects.) The interfacial tension between phases α and β changes its sign at an upsilon point: positive on the first-order line and negative in the mixed-phase region. The phase diagram has a self-similar structure: a part of it looks like the whole; see the magnifications of particular parts of the phase diagram shown as the insets (a) and (b) of Fig. 1. It is noted that every endpoint of first-order lines in the mixed-phase region is also an upsilon point, as suggested by the structures in the leftmost part of Fig. 1 and in the inset (b). A portion of a solid line away from any first-order line has a structure of "devil's staircase;"[13,14] see the insets (c) and (d) of Fig. 1. An upsilon point is an accumulation point of other upsilon points connected through a network of devil's staircases.

An upsilon point is similar to the multiphase points in the ANNNI model,[7] the three-state chiral clock model,[15] the chiral XY model,[16] and a lattice model with a "nonconvex" interaction[17] in that infinitely many phases emerge from a particular point in the phase diagram. But the structure of the phase diagram near an upsilon point is qualitatively different from and much more complicated than those near the multiphase points. If an upsilon point is compared with a quasitricritical point mentioned above, one will find not only a qualitative difference in the phase diagrams near these points, but also a difference in mechanisms which produce these "multicriticalities." A quasitricritical point occurs when a defect pair interaction changes its character from repulsive to attractive,[8,9,11] while it is certain properties of interface interactions, not change in them, that determines the occurrence of an upsilon point.[12]

Examples of upsilon points can be found in certain models of the Frenkevel–Kontorova type.[18–21] Although the analysis of Bassler *et al.*[12] is quite general and not restricted to such models, we know no examples of upsilon points in other models or in real systems. In this paper we shall present evidence that there exist upsilon points in the phase diagram of a spin model which may have some relevance to real magnetic systems.

We consider the one-dimensional system of classical XY spins described by the Hamiltonian

$$\mathscr{H} = \sum_n [-J\cos(\theta_{n+1} - \theta_n) + \cos(\theta_{n+2} - \theta_n) + (K/36)(1 - \cos 6\theta_n) - H\cos\theta_n] \tag{1.1}$$

where θ_n is the angle made by the nth spin vector and an external field whose magnitude is $H > 0$. Each spin interacts with its nearest neighbors through the coupling J and with its next-nearest neighbors antiferromagnetically. The strength of the second-neighbor coupling is chosen as the

unit of energy. The positive parameter K represents the strength of a sixfold anisotropy in the XY plane. The field H is assumed to be applied along one of the easy axes. The model as it is or with further-neighbor spin interactions has been studied in connection with magnetic materials which exhibit layered helical spin configurations.[22]

The ground state of (1.1) with $K=H=0$ is ferromagnetic for $J>4$ and antiferromagnetic for $J<-4$, while a helical spin structure in which

$$\theta_{n+1}-\theta_n=\arccos(J/4) \tag{1.2}$$

is realized for $|J|<4$. In the presence of the magnetic field H but without the anisotropy K, the ground-state phase diagram of (1.1) was constructed by Nagamiya *et al.*[13] based on approximations which are valid at weak and strong fields. According to them, a first-order phase transition from a helical spin structure to another modulated structure, a "fan" structure, occurs as the magnetic field is increased. Further increase of the field results in a continuous (second-order) transition to the ferromagnetic state. The second-order line is given by $H=4(1-J/4)^2$ for $|J|<4$. Kitano and Nagamiya[24] studied the effects of the anisotropy on these phase transitions, using a rather crude approximation.

We are interested in the ground-state phase diagrams of (1.1) in the (J, H) plane for fixed values of K. We begin with the study of an extreme case, i.e., the limit $K=\infty$. In this limit the values available for the spin angle θ becomes discrete and the exact phase diagram can be obtained (Section 3) with the aid of the minimization eigenvalue method introduced by Griffiths and Chou,[25,19] a brief explanation of which is given in the context of the present model in the next section. In Section 4, a part of the phase diagram for finite but large K is studied in the form of a $1/K$ expansion. Candidates for upsilon points are found in the second-order approximation. The interactions between the interfaces whose energies become zero at these points are calculated numerically for moderate values of K in Section 5, since the nature of the interface interactions determines the occurrence of upsilon points. The numerical results indicate the presence of upsilon points in model (1.1). Mixed phases found near these points consist of segments of helical and fan structures, which are analogous to the spin structures discussed by Jensen and Mackintosh[26] in the study of the magnetic structure of the rare-earth metal Ho.

2. MINIMIZATION EIGENVALUE METHOD

Finding the ground state of (1.1) is not a trivial task. We shall employ several methods in order to attack this problem, one of which is described in this section. The other methods will be introduced in Sections 4 and 5.

Griffiths and Chou[25,19] have shown that finding the ground state of (1.1) or a similar one-dimensional model is equivalent to solving a nonlinear eigenvalue equation. In the case of (1.1), the eigenvalue equation is given by

$$\varepsilon + \Psi(\theta, \theta') = V(\theta) + W_1(\theta - \theta') + \min_{\theta''}[W_2(\theta - \theta'') + \Psi(\theta', \theta'')] \quad (2.1)$$

where ε and $\Psi(\theta, \theta')$ are the eigenvalue and eigenfunction; the functions V, W_1, and W_2 are defined by

$$\begin{aligned} V(\theta) &= (K/36)(1 - \cos 6\theta) - H\cos\theta \\ W_1(\phi) &= -J\cos\phi, \qquad W_2(\psi) = \cos\psi \end{aligned} \quad (2.2)$$

Equation (2.1) must be solved for ε and Ψ with the periodic condition

$$\Psi(\theta, \theta') = \Psi(\theta + 2\pi, \theta') = \Psi(\theta, \theta' + 2\pi) \quad (2.3)$$

imposed on Ψ. The eigenvalue ε turns out to be identical with the energy per spin in the ground state of (1.1). The spin configuration of the ground state can be obtained from the map $\tau(\theta, \theta')$, which is defined such that it yields the value of θ'' minimizing the right-hand side of (2.1) for given values of θ and θ'.

Two numerical procedures have been introduced for solving the minimization eigenvalue equation (2.1);[19,27] we shall use one of these or the other, depending on the situation. In the numerical procedures, the continuous variables θ, θ', and θ'' are replaced by discrete ones taking on a total of N values uniformly spaced on the interval $[0, 2\pi)$. The first procedure introduced by Chou and Griffiths[19] is a simple iteration method. Starting with a trial eigenfunction, the iteration stops when the maximum difference between two successive approximate solutions for Ψ becomes less than a predetermined small value δ. With reasonable choices of trial functions and δ, the computer time spent by this procedcure is roughly proportional to N^3. The second procedure, introduced by Floría and Griffiths,[27] applies to the modified version of (2.1), i.e.,

$$2\varepsilon + \Psi(\theta, \theta') = \hat{V}(\theta, \theta') + \min_{\chi, \chi'}[\hat{W}(\theta, \theta', \chi, \chi') + \Psi(\chi, \chi')] \quad (2.4)$$

where

$$\begin{aligned} \hat{V}(\theta, \theta') &= V(\theta) + W_1(\theta - \theta') + V(\theta') \\ \hat{W}(\theta, \theta', \chi, \chi') &= W_2(\theta - \chi) + W_1(\theta' - \chi) + W_2(\theta' - \chi') \end{aligned} \quad (2.5)$$

The computer time for this procedure to find ε and Ψ is roughly proportional to N^4. (It is noted that the computer times necessary for both the methods is of order N^2 for models without second-neighbor interactions.)

Even though the Floría–Griffiths algorithm takes more computer time than the iteration method, there are good reasons to use it. It yields the (numerically) exact answer to the discretized version of (2.4) within a finite number of steps, while the iteration procedure never converges exactly. Another advantage of this method is that the information about interfaces, which play a crucial role in the analysis of the phase diagram, can be obtained (see Section 3.2). For detailed discussion of the minimization eigenvalue equation (2.1) and the numerical procedures for solving it, the reader is referred to the original papers[19,25,27] and the review article by Griffiths[28]

3. THE LIMIT $K = \infty$

3.1. Phase Diagram

In the limit of strong anisotropy ($K = \infty$), the spin angle θ can only take on discrete values:

$$\theta = k\pi/3 \qquad (k = 0, 1, 2, 3, 4, \text{ or } 5) \tag{3.1}$$

Thus the model reduces to a six-state clock model, the integer k being the "clock variable." Then the Floría–Griffiths algorithm (with $N = 6$) discussed in the previous section can be used to obtain the exact ground state of (1.1) for given values of J and H.

The phase diagram obtained in this limiting case is shown in Fig. 2. It

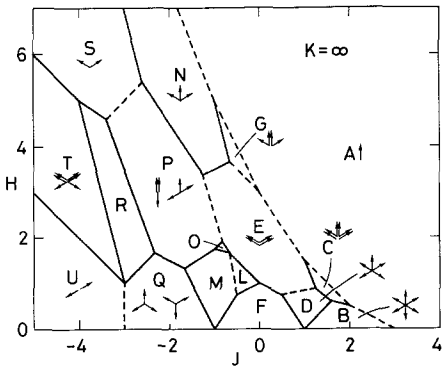

Fig. 2. The phase diagram in the strong anisotropy limit ($K = \infty$). The solid and dashed phase boundaries represent superdegenerate and first-order lines.

consists of 17 regions, representing phases A–G and L–U, separated by the phase-transition lines or phase boundaries. The dashed lines represent first-order transitions as in Fig. 1, but the solid lines here and henceforth have a different meaning from that in Fig. 1: each of the solid lines indicates a single phase transition, not a collection of transitions, with certain properties explained in the next subsection. The three transition lines between phases A and S (not shown in the figure), S and T, and T and U are parallel to each other and extend to infinity. The spin configurations for some of the phases are shown in Fig. 2 by the directed arrows. Phase A is ferromagnetic and U antiferromagnetic. On the line $H=0$, modulated spin structures other than the ferro- or antiferromagnetic states exist for $|J|<3$. This interval is somewhat shorter than that in the isotropic case ($|J|<4$) discussed in the introduction.

All the spin configurations found in the ground states for $K=\infty$ are periodic, the maximum period being 12 of phase L. A periodic configuration can be specified by giving the sequence of clock variables k, defined in (3.1), in a period. We put this sequence in angular brackets. For example,

Table I. The Spin Configurations and the Energies per Spin for the Phases Appearing in Fig. 2

Phase	Spin configuration	Energy per spin
A	$\langle 0 \rangle$	$1-J-H$
B	$\langle 012345 \rangle$	$-(1+J)/2$
C	$\langle 011055 \rangle$	$(1-4J-4H)/6$
D	$\langle 01245 \rangle$	$-(7+3J+2H)/10$
E	$\langle 1155 \rangle$	$-(2+J+2H)/4$
F_1	$\langle 1144 \rangle$	-1
F_2	$\langle 1245 \rangle$	-1
F_3	$\langle 0033 \rangle$	-1
F_4	$\langle 0134 \rangle$	-1
G	$\langle 0105 \rangle$	$(1-2J-3H)/4$
L	$\langle 145125521541 \rangle$	$-(10-J+2H)/12$
M	$\langle 0135024 \rangle$	$-(11-3J+2H)/14$
N	$\langle 015 \rangle$	$(1-J-4H)/6$
O	$\langle 0145125024 \rangle$	$-(7-2J+2H)/10$
P_1	$\langle 003 \rangle$	$-(1-J+H)/3$
P_2	$\langle 014 \rangle$	$-(1-J+H)/3$
Q_1	$\langle 024 \rangle$	$-(1-J)/2$
Q_2	$\langle 135 \rangle$	$-(1-J)/2$
R	$\langle 02514 \rangle$	$(3+7J-2H)/10$
S	$\langle 15 \rangle$	$(2+J-H)/2$
T	$\langle 141525 \rangle$	$(4+5J-H)/6$
U	$\langle 14 \rangle$	$1+J$

the structure of phase C is represented by $\langle 011055 \rangle$. The spin configurations for all the phases appearing in Fig. 2 are summarized in Table I, along with the expression for the energy per spin for each phase, from which the phase boundaries can be calculated. The ground states for phases F, P, and Q are degenerate.

Phases B, Q_1, and Q_2 show *helical* spin structures, while the structures of D, F_2, M, and some others are deformed helices. A helix, deformed or not, can be right-handed or left-handed; e.g., phase D can be either $\langle 01245 \rangle$ or $\langle 54210 \rangle$. The energy of a helical structure is independent of its handedness because the Hamiltonian (1.1) is invariant under the transformation $\theta_n \to \theta_{-n}$. Phases C, E, and G and some others may be regarded as having *fan* structures, in which the spin direction oscillates about the direction of the magnetic field as one moves along the chain.

Since it is impossible to numerically solve the eigenvalue equation (2.4) for *every* pair of J and H, there might be some phases missed in Fig. 2. However, we believe that Fig. 2 is the exact phase diagram for $K = \infty$ for the following reason. First of all, we note that the energy per spin ε of any configuration is a linear function of J and H in this limiting case, as explicitly seen in the third column of Table I. This is because the direction of each spin is fixed by the infinitely strong anisotropy and does not change when J and H are varied. The linear dependence of ε on J and H implies that each region appearing in the phase diagram has the shape of a convex polygon. Therefore, if there were phases missed in Fig. 2, one could find those phases by solving (2.4) in the vicinity of a point in the phase diagram where two or more lines (phase boundaries or the line $H = 0$) come together. We have found no extra phases by such inspection.

3.2. Superdegenerate Lines

There are two types of phase-transition lines in Fig. 2: first-order lines indicated by the dashed lines and *superdegenerate* lines indicated by the solid lines. The distinction arises from the properties of an interface between the two phases coexisting on a phase boundary. On a first-order line, the creation energy of an interface has a positive value. On a superdegenerate line, the interface energy and the interactions between interfaces are zero.[7,9,12] In the latter situation, interfaces can be brought into the system without extra cost of energy. Therefore, various sorts of structures consisting of segments of one phase and the other separated by interfaces between them can be the ground state: the ground state is infinitely degenerate.

The distinction between the first-order and superdegenerate lines is important[9,12] for the analysis of the phase diagram at finite, large K,

where the parameter $1/K$ can be considered as a small perturbation. A small perturbation can remove the degeneracy at a superdegenerate line, and qualitative changes in the phase diagram may result. By contrast, no qualitative change will occur at a first-order line by a small perturbation.

Given two phases, there can be more than one type of interface between them. The one with the lowest creation energy is the one referred to in the above discussion. As an example, the minimum energy interface between phases E and G is shown in Fig. 3a, where the spin configuration is represented by a sequence of clock variables, and the single and double underlines are used to denote regions belonging to different phases. The interface show in Fig. 3b is not the minimal one. The minimum energy interface at a given phase transition may be found with the aid of the eigenfunctions Ψ of (2.1) associated with one phase and the other.[28] When the ground state is degenerate, the Floria–Griffiths algorithm for solving (2.4) can be used to find Ψ for each of the distinct ground states,[27,20] whereas the iteration procedure tends to obtain a "mixed" Ψ composed of parts belonging to different Ψ associated with different pure phases.[19] Therefore, the latter procedure is not suited for finding the minimum energy interface at a phase transition.

In order to calculate the creation energy of an interface, a spin configuration containing a pair of interfaces needs to be considered.[7,9,12,29] In Fig. 3c, such a configuration with interfaces of the type shown in Fig. 3a is presented. Let θ_{-i} and θ_j be the angles of spins located far to the left and right, respectively, of the interface pair, and assume that the integers i and j are chosen such that the equality $\theta_{-i}=\theta_j$ holds if i and j are large enough. Then the formula

$$\lim_{i,j\to\infty} \sum_{n=-i}^{j-1} [V(\theta_n)+W_1(\theta_{n+1}-\theta_n)+W_2(\theta_{n+2}-\theta_n)-\varepsilon_\alpha] = 2\sigma+\phi_\beta(m) \tag{3.2}$$

can be used to calculate the creation energy σ of the interface. In this formula, ε_α is the energy per spin for the pure phase which lies outside the

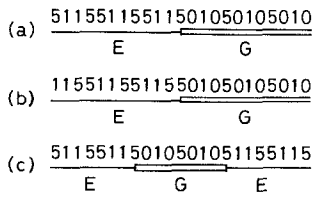

Fig. 3. Spin configurations with interfaces between phases E and G: (a) the minimum-energy interface; (b) an interface whose energy is not minimal; (c) a pair of the minimum-energy interfaces separated by the distance 8.

interface pair (phase E in the case of Fig. 3c) and $\phi_\beta(m)$ represents the interaction between the two interfaces, which are assumed to be separated by a distance m ($m=8$ in the case of Fig. 3c). Assuming that $\phi_\beta(m) \to 0$ as $m \to \infty$, σ is obtained from (3.2) by this limiting process. Once σ is determined, (3.2) is used to define $\phi_\beta(m)$ for finite m. For the example shown in Fig. 3c, we have $\sigma = (2+3J)/8$ and $\phi_\beta(m) = 0$ on the phase boundary, $J+H=3$ $(-2/3 < J < 0)$, between phases E and G. The interface given in Fig. 3b has a creation energy $\sigma = (2-3J)/8$, which is larger than the previous one.

The definitions of the interaction energies associated with more than two interfaces are given in ref. 12, which are straightforward extensions of multidefect interactions defined by Fisher and Szpilka.[9] It turns out that all the interactions associated with the minimum energy interfaces on the phase-transition lines in Fig. 2 are zero.

4. EXPANSION IN POWERS OF $1/K$

We now consider modifications of the phase diagram, Fig. 2, produced by reducing the anisotropy K from infinity to a finite value. For finite K, the spin angle θ can be any value in the interval $[0, 2\pi)$. In order to obtain the phase diagram with reasonable accuracy by numerically solving the eigenvalue equation (2.1), one needs to work with a somewhat large N (a few hundred or more), the number of grid points in the discretization of θ; this method will take much computer time. In this section we shall consider an analytic approach, which can be used in the case of large K, to keep the amount of numerical work we need as small as possible. The method described below is somewhat analogous to the low-temperature expansions used by Fisher and Selke[7] and Fisher and Szpilka[8–11] in the study of the phase diagrams for the ANNNI and chiral clock models.

The spin configuration $\{\theta_n\}$ in the ground state or a metastable state, which may contain a number of interfaces, satisfies the force equilibrium condition

$$\partial \mathscr{H}/\partial \theta_n = 0 \tag{4.1}$$

If the anisotropy K is large, the direction of a spin vector will not deviate very much from one of the easy axes. That is, the angle φ_n defined by

$$\theta_n = k_n \pi/3 + \varphi_n \tag{4.2}$$

is small in a force equilibrium configuration for large K. In (4.2), k_n is one of the clock variables (integers 0–5). If a set of integers $\{k_n\}$ is given, the deviation angles φ_n in the corresponding equilibrium configuration are

found by solving (4.1). Since every φ_n vanishes as $K \to \infty$, it may be obtained in the form

$$\varphi_n = \frac{1}{K}\varphi_n^{(1)} + \frac{1}{K^2}\varphi_n^{(2)} + \cdots \tag{4.3}$$

Substituting (4.2) with (4.3) into (4.1), we find

$$\begin{aligned}\varphi_n^{(1)} = &-H \sin\theta_n^{(0)} + J[\sin(\theta_{n+1}^{(0)} - \theta_n^{(0)}) - \sin(\theta_n^{(0)} - \theta_{n-1}^{(0)})] \\ &- \sin(\theta_{n+2}^{(0)} - \theta_n^{(0)}) + \sin(\theta_n^{(0)} - \theta_{n-2}^{(0)})\end{aligned} \tag{4.4}$$

from the terms lowest order in $1/K$, where $\theta_n^{(0)} = k_n\pi/3$. From the next-order terms, the following equations for $\varphi_n^{(2)}$ is obtained:

$$\begin{aligned}\varphi_n^{(2)} = &-H\varphi_n^{(1)} \cos\theta_n^{(0)} \\ &+ J[(\varphi_{n+1}^{(1)} - \varphi_n^{(1)}) \cos(\theta_{n+1}^{(0)} - \theta_n^{(0)}) - (\varphi_n^{(1)} - \varphi_{n-1}^{(1)}) \cos(\theta_n^{(0)} - \theta_{n-1}^{(0)})] \\ &- (\varphi_{n+2}^{(1)} - \varphi_n^{(1)}) \cos(\theta_{n+2}^{(0)} - \theta_n^{(0)}) + (\varphi_n^{(1)} - \varphi_{n-2}^{(1)}) \cos(\theta_n^{(0)} - \theta_{n-2}^{(0)})\end{aligned} \tag{4.5}$$

The energy E associated with a spin configuration $\{\theta_n\}$ in force equilibrium is calculated by substituting $\{\theta_n\}$ into (1.1). After some manipulations, noting the relations (4.4) and (4.5), one finds the formula

$$E = E_0 - \frac{1}{2K}\sum_n (\varphi_n^{(1)})^2 - \frac{1}{2K^2}\sum_n \varphi_n^{(1)}\varphi_n^{(2)} + O\left(\frac{1}{K^3}\right) \tag{4.6}$$

where E_0 is the energy of the system for $K = \infty$. We shall calculate, using this formula, the energies for various spin configurations which are relevant to the analysis of the phase diagram.

As noted in Section 3.2, qualitative changes in the phase diagram due to the finiteness of K can occur at superdegenerate lines in Fig. 2. We shall concentrate our attention on three of these lines: the lines separating phases B, C, and D, which come together at the point $(J, H) = (8/5, 3/5)$. In order to see whether new phase regions appear in the phase diagram, the interface energies are calculated at these superdegenerate lines. The interfaces of interest are those shown in Fig. 4. In this figure, spin configurations are represented by sequences of clock variables k_n, but this does not mean that the spins are parallel to the easy axes; it is understood that the orientation θ_n of each spin deviates slightly from the easy axis implied by the integer k_n by an amount determined by (4.1). The same remark applies to similar representations, which will appear in what follows, e.g., (4.9) and Fig. 6 below.

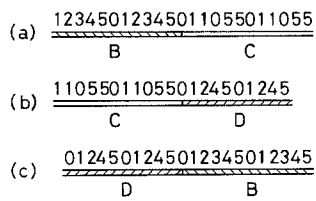

Fig. 4. The minimum-energy interfaces connecting (a) phases B and C, (b) C and D, (c) D and B.

In the first-order calculation, it is found that the creation energies of all the three interfaces shown in Fig. 4 and the interactions between them are zero at the corresponding phase boundaries. Thus, the superdegenerate lines under consideration remain superdegenerate in this approximation. The point at which these lines come together shifts to the location $(J, H) = (J_0, H_0)$, where

$$J_0 = \frac{8}{5} - \frac{9}{125K}, \qquad H_0 = \frac{3}{5} + \frac{69}{500K} \tag{4.7}$$

In the second-order approximation, the creation energy σ_{CD} of the interface between phases C and D is obtained as

$$\sigma_{CD} = -\frac{3}{16K^2}(J-1)^2 \tag{4.8}$$

under the condition that the energies per spin in these phases are the same ($\varepsilon_C = \varepsilon_D$). The fact that σ_{CD} is negative implies the emergence of a new phase which will occupy a finite area in the refined phase diagram.[7,9] Since it turns out that the interactions between the interfaces are absent in this approximation, the new phase has the structure in which interfaces between phases C and D are packed as closely as possible, i.e., the structure represented by

$$\langle 0124501105421055 \rangle \tag{4.9}$$

whose period is 16. In this structure, there are four interfaces in each period. This new phase will be called phase CD.

The structure (4.9) may be represented in a more compact way, because the second half of the configuration in a period is the "mirror image" of the first half: $\theta_{n+8} = -\theta_n \pmod{2\pi}$. We shall represent the spin configuration (4.9) of phase CD as

$$\langle 01245011 \rangle^2 \tag{4.10}$$

for short. The general definition of the new notation is as follows:

$$\langle k_1 k_2 \cdots k_r \rangle^2 = \langle k_1 k_2 \cdots k_r \bar{k}_1 \bar{k}_2 \cdots \bar{k}_r \rangle \tag{4.11}$$

where r is half the period of the structure and $\bar{k}_n = 6 - k_n \pmod 6$. This convention could have been used to represent some of the configurations in Table I, e.g., $\langle 011 \rangle^2$ for phase C.

The creation energies of the other interfaces shown in Fig. 4 are also found to be negative in the second-order approximation:

$$\sigma_{BC} = -\frac{3}{16K^2}(J-2)^2, \qquad \sigma_{DB} = -\frac{3}{16K^2} \tag{4.12}$$

where σ_{BC} and σ_{DB} are the energies of the interfaces between phases B and C and phases D and B. The interface interactions are absent in the same approximation. The structures of the new phases BC and DB, which will appear between phases B and C and between phases D and B in the refined phase diagram, are respectively given by

$$\langle 012345011 \rangle^2 \qquad \text{and} \qquad \langle 01245012345 \rangle \tag{4.13}$$

There are two interfaces in each half of the period in the former structure and in each period in the latter.

It is noted that both right-handed and left-handed helices (segments 01245 and 05421) are building blocks of the structure of phase CD, (4.9). These blocks are connected via a segment of fan structure (011 or 055). The same is true for the structure of phase BC, the helical segments in this case being 012345 and 054321. These structures are analogous to what Jensen and Mackintosh[26] called "helifan" in their study of the magnetic structure of Ho. The structure of the other new phase, DB, is a helix with a definite handedness.

The phase diagram in the second-order approximation near the point where three phases B, C, and D come together in the first-order approximation is obtained by comparing the energies per spin for these three phases and the three new phases. The result is shown in Fig. 5 as the phase diagram in the (x, y) plane, where the parameters x and y are shifted and rescaled versions of J and H:

$$x = (J - J_0)K^2, \qquad y = (H - H_0)K^2 \tag{4.14}$$

where J_0 and H_0 are given in (4.7). In this phase diagram, the solid and dashed lines indicate superdegenerate and first-order lines as in Fig. 2; the nature of the phase transitions has been determined from the creation energies of appropriate interfaces and interactions between them calculated

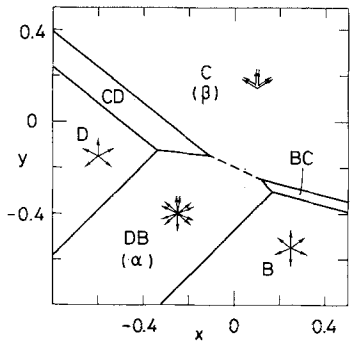

Fig. 5. A portion of the phase diagram obtained in the second-order approximation of the $1/K$ expansion. The parameters x and y are defined in (4.14).

in the second-order approximation. The locations of the three phase points in Fig. 5 are listed in Table II.

In what follows, the helical phase DB and the fan phase C will be referred to as phases α and β for convenience. On the left half of the first-order line between these phases, the interface shown in Fig. 6a has the minimum creation energy. The energy σ_1 of this interface, which will be called interface I_1, evaluated on the first-order line $(17x+38y+4668/5^4=0)$ is given by

$$\sigma_1=\frac{15}{38K^2}\left(\frac{1409}{4\cdot 5^5}+x\right) \tag{4.15}$$

which vanishes at the left end of the transition line and becomes negative

Table II. The Locations of the Three Phase Points in Fig. 5

Point	x	y
$B:BC:DB$	$\frac{2091}{4\cdot 5^5}$	$-\frac{7653}{8\cdot 5^5}$
$C:BC:DB$	$\frac{1441}{4\cdot 5^5}$	$-\frac{6203}{8\cdot 5^5}$
$C:CD:DB$	$-\frac{1409}{4\cdot 5^5}$	$-\frac{3653}{8\cdot 5^5}$
$D:CD:DB$	$-\frac{8443}{8\cdot 5^5}$	$-\frac{6181}{16\cdot 5^5}$

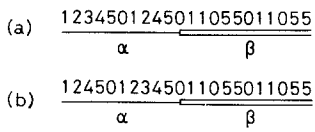

Fig. 6. Interfaces (a) I_1 and (b) I_2 between phases α and β.

beyond this point. The interface shown in Fig. 6b, which will be called interface I_2, has the creation energy

$$\sigma_2 = \frac{15}{38K^2}\left(\frac{1441}{4\cdot 5^5} - x\right) \tag{4.16}$$

which is smaller than σ_1 on the right half of the α–β phase boundary. The value of σ_2 goes to zero at the right end of the transition line and becomes negative beyond it.

It is interesting to note that the structure of phase CD can be viewed as consisting of close-packed interfaces I_1, shown in Fig. 6a, between phases α and β (that is, phases DB and C), even though this structure was found by packing interfaces between phases C and D as densely as possible. This observation and the fact that the first-order coexistence of α and β terminates at the point where $\sigma_1 = 0$ bring us to the starting point of the analysis by Bassler *et al.*,[12] which is a straightforward but nontrivial extension of the work by Fisher and Szpilka.[9] According to their theory, the nature of the interactions between interfaces I_1, which is absent in the present approximation but will be present in refined calculations, determines the fine structure of the phase diagram near the endpoint of the first-order line. The same argument with interface I_2 in place of I_1 applies to the other endpoint of the α–β transition.

5. EVIDENCE FOR UPSILON POINTS

In this section we shall study the detailed structure of the phase diagram, which will be revealed by refined calculations, near the endpoints of the first-order line between phases α and β in Fig. 5, using the strategy employed by Bassler *et al.*[12] We first consider the left end of the α–β transition, where the energy σ_1 of interface I_1 shown in Fig. 6a vanishes in the second-order approximation of the $1/K$ expansion. The structures of phases which might appear near this point in the phase diagram upon further refinement of calculation consist of segments of phases α and β with interfaces I_1 inserted between them; an example of such structures is the configuration (4.9) or (4.10) for phase CD. It is noted that the size (the

number of spins contained) l of a segment of phase α can only take on the values

$$l = 5 + 11p \tag{5.1}$$

where $p \geqslant 0$ is any nonnegative integer. Similarly, the size m of a segment of phase β takes on the values

$$m = 3 + 3q \tag{5.2}$$

where $q \geqslant 0$ is any nonnegative integer.

The spin configuration for any of these "mixed phases" can be identified by a set of integers $\{l_i, m_i\}$, representing the sequence of segment lengths. We adopt the convention introduced by Bassler *et al.*[12] to denote periodic configurations: a sequence of segment lengths l and m in a period is put in square brackets (an l always comes first and an m last). For example, the configuration (4.9) for phase CD is denoted as $[5, 3, 5, 3]$. In this example (and others to come), where the second half of the configuration in a period is the "mirror image" of the first half, we can use the shorter notation $[5, 3]^2$ in analogy to (4.10).

The energy E associated with a mixed phase can be expressed as[9,12]

$$E = \sum_i [2\sigma_1 + l_i \varepsilon_\alpha + m_i \varepsilon_\beta] + \Phi \tag{5.3}$$

where ε_α and ε_β are the energies per spin in phases α and β, and Φ is the sum of the interface interactions:

$$\begin{aligned} \Phi = \sum_i [&\phi_\alpha(l_i) + \phi_\beta(m_i) + \phi_\alpha(l_i, m_i) \\ &+ \phi_\beta(m_i, l_{i+1}) + \phi_\alpha(l_i, m_i, l_{i+1}) + \cdots] \end{aligned} \tag{5.4}$$

The first (second) term in the brackets of (5.4) is the interaction between a pair of interfaces between which lies a segment of phase α (β) of length l_i (m_i). The third term represents the three-body interaction associated with three consecutive interfaces, the first interface being followed by a segment α of size l_i and the second one by a segment β of size m_i. Now the meaning of the other terms in (5.4) should be clear. As noted in Section 3.2, the precise definitions of the multibody interactions are given in refs. 12 and 9. In the strategy of Bassler *et al.*[12] (and of Fisher and Szpilka[9]), we first neglect all interface (defect) interactions and then successively take into account the pair, triplet, and higher-order interactions to systematically construct the phase diagram.

We have calculated the two- through six-body interactions based on the numerical solutions of the force equilibrium equation (4.1) for various configurations containing interfaces. It turns out that the interaction decreases rapidly with the number of interfaces and with the distances between interfaces. The results for the pair interactions $\phi_\alpha(l)$ and $\phi_\beta(m)$ are shown in Fig. 7, which are obtained for $K=1.5$ under the condition that $\varepsilon_\alpha=\varepsilon_\beta$ and $\sigma_1=0$ (this implies $J\approx 1.55268$, $H\approx 0.65929$). The values of $\phi_\alpha(l)$ and $\phi_\beta(m)$ for given l and m change very little over the small ranges of J and H we are interested in, while they get small rapidly as the anisotropy K is increased. Both $\phi_\alpha(l)$ and $\phi_\beta(m)$ are positive for all $l\geqslant 5$ and $m\geqslant 3$, and satisfy the *convexity conditions*

$$\Delta^2\phi_\alpha(l)=\phi_\alpha(l+11)+\phi_\alpha(l-11)-2\phi_\alpha(l)>0 \tag{5.5}$$

$$\Delta^2\phi_\beta(m)=\phi_\beta(m+3)+\phi_\beta(m-3)-2\phi_\beta(m)>0 \tag{5.6}$$

for all $l>5$ and $m>3$. The three-body interaction $\phi_\alpha(l, m)$ calculated with the same values of K, J, and H used for Fig. 7 is plotted in Fig. 8a. The *double difference* $\Delta^2\phi_\alpha(l, m)$ of the three-interface interaction defined by the following equation is *positive* for $l\geqslant 5$ and $m\geqslant 3$:

$$\Delta^2\phi_\alpha(l, m)=\phi_\alpha(l, m)+\phi_\alpha(\bar{l}, \bar{m})-\phi_\alpha(\bar{l}, m)-\phi_\alpha(l, \bar{m}) \tag{5.7}$$

where $\bar{l}=l+11$ and $\bar{m}=m+3$. It turns out that $\phi_\alpha(l, m)=\phi_\beta(m, l)$ for any l and m, and therefore the equality $\Delta^2\phi_\beta(m, l)=\Delta^2\phi_\alpha(l, m)$ holds for $\Delta^2\phi_\beta(m, l)$ defined by (5.7) with α, l, and m replaced by β, m, and l. The importance of the convexity, or lack thereof, of pair interactions and the sign of the double differences of three-body interactions was first recognized by Fisher and Szpilka.[9]

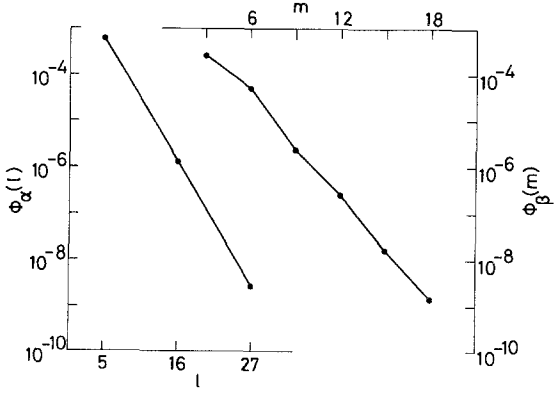

Fig. 7. The pair interactions $\phi_\alpha(l)$ and $\phi_\beta(m)$ for interface I_1, shown in Fig. 6a, calculated for $K=1.5$, $J=1.5526796095$, and $H=0.6592867195$.

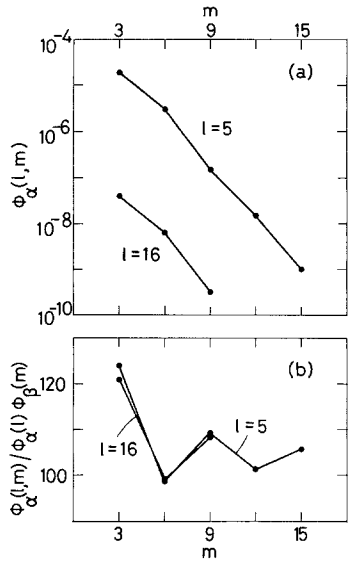

Fig. 8. (a) The three-body interaction $\phi_\alpha(l, m)$ for interface I_1 calculated with the same values of K, J, and H used for Fig. 7. (b) The plot of the ratio $\phi_\alpha(l, m)/\phi_\alpha(l)\,\phi_\beta(m)$ implies the asymptotic factorization formula (5.9).

In the approximation which neglects the interactions associated with four or more interfaces, the qualitative features of the phase diagram are determined by the signs of $\Delta^2\phi_\alpha(l)$, $\Delta^2\phi_\beta(m)$, $\Delta^2\phi_\alpha(l, m)$, and $\Delta^2\phi_\beta(m, l)$. They are all positive in the present case. This fact implies[12] that the phase diagram consists of the regions representing phases $[l, m]$ (or $[l, m]^2$ if m is given by (5.2) with even q) with any combinations of $l \geqslant 5$ and $m \geqslant 3$. The phase diagram obtained for $K = 1.5$ is shown in Fig. 9. The phase transitions between $[l, \bar{m}]$ and $[\bar{l}, m]$ are of first order; the lengths of the transition lines get smaller with the values of l and m. The other transition lines are superdegenerate, except, of course, for the line between α and β. The locations of the phase-transition lines in Fig. 9 are obtained by numerically comparing the energies per spin for different phases. They can also be calculated by using the formulas given in ref. 12, which are expressed in terms of ε_α, ε_β, σ_1, and the interface interactions.

Since Fig. 9 is full of superdegenerate lines, the higher-order interface interactions can yield qualitative changes in the phase diagram. The effects of the four- and five-body interactions are examined by using the "renormalization" procedure explained in ref. 12. It turns out that these interactions lead to splitting of the superdegenerate lines in Fig. 9 to produce mixed phases of more complicated structures. The resulting phase diagram

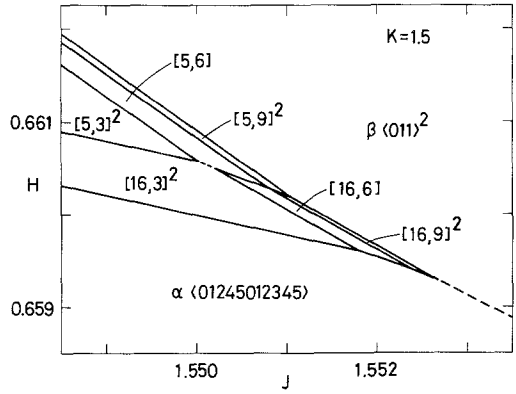

Fig. 9. The phase diagram near the left endpoint of the first-order line between phases α and β.

near the left endpoint of the first-order line between phases [5, 6] and $[16, 3]^2$ is shown in Fig. 10. Note that the scale of this figure is magnified 300 times compared to that of Fig. 9; the effects of the four- and five-interface interactions are so small that they do not show up in the phase diagram presented with the scale of Fig. 9.

The structure of Fig. 10 resembles that of Fig. 9. Then, is it expected that the superdegenerate lines in Fig. 10 will split due to still higher-order interactions to produce structures resembling Figs. 9 or 10 in finer scales? If such splittings continue indefinitely, the resulting phase diagram has a *self-similar* structure. If this is the case, the endpoint of the α–β transition line in Fig. 9 is an *upsilon point*[12] explained in the introduction (the

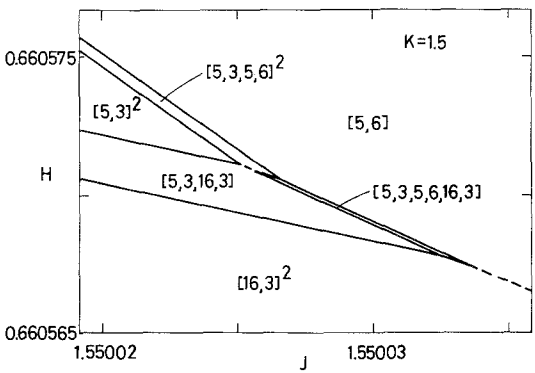

Fig. 10. A portion of the phase diagram of Fig. 9, near the left end of the first-order line between phases [5, 6] and $[16, 3]^2$, is presented with 300-fold magnification.

endpoints of the other first-order lines in Fig. 9 and those in Fig. 10 are also upsilon points).

One cannot be certain, with numerical results of finite accuracy, whether the splittings of the superdegenerate lines continue endlessly. Nevertheless, we find evidence that the end endpoint of the first-order line between phases α and β is an upsilon point. We first note that, as can be seen from Fig. 7, the pair interactions $\phi_\alpha(l)$ and $\phi_\beta(m)$ for large l and m are well described by the exponential formulas

$$\phi_\alpha(l) = C_\alpha \Lambda_\alpha^p, \qquad \phi_\beta(m) = C_\beta \Lambda_\beta^q \tag{5.8}$$

where p and q are related to l and m through (5.1) and (5.2), respectively, and C_α, Λ_α, C_β, and Λ_β are positive constants ($C_\alpha \approx 6 \times 10^{-4}$, $\Lambda_\alpha \approx 2.1 \times 10^{-3}$, $C_\beta \approx 5 \times 10^{-4}$, and $\Lambda_\beta \approx 7.8 \times 10^{-2}$ for the case shown in Fig. 7). The next observation is that the ratio $\phi_\alpha(l, m)/\phi_\alpha(l)\,\phi_\beta(m)$ approaches a constant value as l and m are increased; see Fig. 8b. This fact implies that the factorization formula

$$\phi_\alpha(l, m) = \phi_\beta(m, l) = t\phi_\alpha(l)\,\phi_\beta(m) \tag{5.9}$$

holds for large l and m, where t is a positive constant ($t \approx 1.03 \times 10^2$ for the case shown in Fig. 8). Furthermore, our numerical results for interactions involving up to six interfaces show that the factorization rule applies to the higher-order interface interactions as well if the separations between interfaces are large:

$$\begin{aligned} \phi_\alpha(l_1, m_1, l_2, \ldots) &= \phi_\alpha(l_1)\, t\phi_\beta(m_1)\, t\phi_\alpha(l_2)\ldots \\ \phi_\beta(m_1, l_1, m_2, \ldots) &= \phi_\beta(m_1)\, t\phi_\alpha(l_1)\, t\phi_\beta(m_2)\ldots \end{aligned} \tag{5.10}$$

where the number of factors t on the right-hand side of each equation is one less than the number of arguments of ϕ on the left. We speculate that the (asymptotic) factorization rule holds for *all* the interface interactions. If the interactions have this property as well as the exponential form (5.8), we are certain that the left endpoint of the first-order line between phases α and β is an upsilon point (see Section 8 of ref. 12 for detailed explanation).

Apart from the factors C and t and the values of Λ in (5.8)–(5.10), the exponential form of the pair interactions and the factorization of the multibody interactions can be inferred from the general argument by Fisher and Szpilka[9] for models with short-range interactions. However, the information obtained from this general argument is not enough to decide whether the point considered here is an upsilon point. The crucial facts revealed by the numerical calculation discussed in the previous paragraph are that the factorization formulas (5.10) contain only those constants which appear in

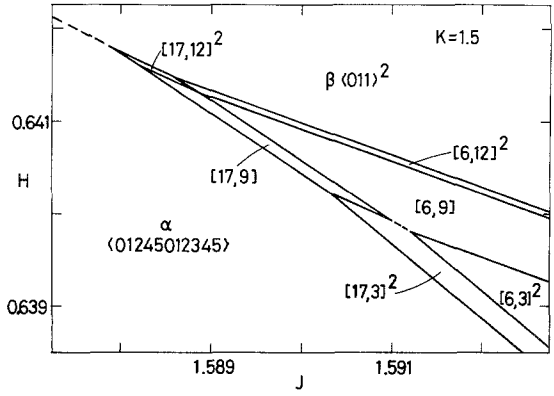

Fig. 11. The phase diagram near the right endpoint of the first-order line between phases α and β.

the pair and triplet interactions (C_α, C_β, Λ_α, Λ_β, and t) and that all of these constans are positive.

Now we turn our attention to the right end of the α–β transition line, where the energy σ_2 of interface I_2 shown in Fig. 6b becomes zero. The mixed phases which can be stable near this point consist of segments of phases α and β separated by interfaces I_2. The lengths l and m of phases α and β can take on the values

$$l = 6 + 11p, \qquad m = 3 + 3q \tag{5.11}$$

with any nonnegative integers p and q. We have numerically calculated the interactions between interfaces I_2, up to six-body interactions. The results are qualitatively the same as those for interfaces I_1 described in the preceding paragraphs, which implies that the right endpoint of the α–β transition is an upsilon point, too. The phase diagram obtained near this point is shown in Fig. 11, where phase $[6, 3]^2$ is identical to the one denoted as BC before.

6. CONCLUDING REMARKS

We have provided evidence that there are upsilon points, multicritical points of a new class discussed by Bassler *et al.*,[12] in the ground-state phase diagram of the spin model (1.1). The evidence is obtained from the numerical analysis in the previous section, which is based on the result of the $1/K$ expansion of the second order in Section 4. However, it is true that for sufficiently small anisotropy K the phase diagram possesses features that are not expected from the $1/K$-expansion approach. For example, we

know that the phase transition from the ferromagnetic phase to a fan phase is of second order when K is small enough.[23,24] This result cannot be obtained by the $1/K$-expansion procedure, because the first-order boundary of the ferromagnetic phase in Fig. 2 remains first order when a small perturbation $1/K$ is introduced. Then, to what extent can the $1/K$-expansion result be extrapolated? In particular, is it valid for K as small as 1.5, for which most of the numerical calculations in Section 5 are carried out?

In order to check whether unexpected phases exist in the region of the (J, H) plane considered in the analysis in Section 5, we have solved the minimization eigenvalue equation (2.1) for $K=1.5$ using the Chou–Griffiths iteration algorithm[19] with grid points of $N=120$. The grid is not fine enough to reveal the detailed structures of the phase diagrams presented in Section 5, Figs. 9–11, but the result is consistent with the one obtained in the second-order approximation of the $1/K$ expansion, Fig. 5; no unexpected phases are found. Thus, we conclude that the $1/K$-expansion result can be extrapolated to values of K as small as 1.5, at least for the region of the (J, H) plane investigated here, and therefore the phase diagrams obtained in the last section are correct.

A crucial point for claiming the existence of upsilon points is whether the factorization rule (5.10) really holds for all the interface interactions. For models of the Frenkel–Kontorova type, which include XY spin models, with nearest-neighbor interactions, it has been shown analytically that the factorization rule holds asymptotically with exponentially small corrections for large separations between interfaces.[30] A similar analytic study for models with next-nearest-neighbor interactions would lead to a definite conclusion on the existence of upsilon points in model (1.1).

We have explored only a small portion of the phase diagram for finite K, whereas the complete phase diagram for $K=\infty$ is obtained. In order to construct the complete phase diagram for finite K (in particular for small K), extensive numerical work would be necessary. It is anticipated that interesting features other than the upsilon point, such such as the singular-continuous endpoint, described by Bassler *et al.*,[12] would be revealed by such work.

As pointed out in the introduction and in Section 4, the mixed phases which appear near the endpoints of the first-order transition between the helical phase α and the fan phase β are analogous to what Jensen and Mackintosh[26] proposed for the magnetic structure of Ho in the field. This analogy may suggest a possibility that a careful examination of the magnetic phase diagrams of Ho or some other materials showing helical spin ordering may reveal features characteristic of an upsilon point, although it is noted that the helical structure of phase α here does not seem to be identical to any of the commensurate spin structures observed in Ho.

REFERENCES

1. P. Bak, *Rep. Prog. Phys.* **45**:587 (1982).
2. V. L. Pokrovsky and A. L. Talapov, *Theory of Incommensurate Crystals* (Harwood, New York, 1984).
3. W. Selke, *Phys. Rep.* **170**:213 (1988).
4. J. Yeomans, in *Solid State Physics*, Vol. 41, H. Ehrenreich and D. Turnbull, eds. (Academic Press, New York, 1988), p. 151.
5. W. Selke, in *Phase Transitions and Critical Phenomena*, C. Domb and J. L. Lebowitz, eds. (Academic Press, New York), to appear.
6. J. Villiain and M. B. Gordon, *J. Phys. C* **13**:3117 (1980).
7. M. E. Fisher and W. Selke, *Phys. Rev. Lett.* **44**:1502 (1980); *Phil. Trans. R. Soc. Lond. A* **302**:1 (1981).
8. A. M. Szpilka and M. E. Fisher, *Phys. Rev. Lett.* **57**:1044 (1986).
9. M. E. Fisher and A. M. Szpilka, *Phys. Rev. B* **36**:644 (1987).
10. M. E. Fisher and A. M. Szpilka, *Phys. Rev. B* **36**:5343 (1987).
11. A. M. Szpilka and M. E. Fisher, *Phys. Rev. B* **36**:5363 (1987).
12. K. E. Bassler, K. Sasaki, and R. B. Griffiths, *J. Stat. Phys.* **62**:45 (1991).
13. S. Aubry, in *Solitons and Condensed Matter Physics*, A. R. Bishop and T. Schneider, eds. (Springer, Berlin, 1978), p. 264.
14. B. B. Mandelbrot, *The Fractal Geometry of Nature* (Freeman, New York, 1983).
15. J. M. Yeomans and M. E. Fisher, *J. Phys. C* **14**:L835 (1981).
16. C. S. O. Yokoi, L. H. Tang, and W. Chou, *Phys. Rev. B* **37**:2173 (1988).
17. M. Marchand, K. Hood, and A. Caillé, *Phys. Rev. Lett.* **58**:1660 (1987); *Phys. Rev. B* **37**:1898 (1988).
18. S. Aubry, F. Axel, and F. Vallet, *J. Phys. C* **18**:753 (1985).
19. W. Chou and R. B. Griffiths, *Phys. Rev. B* **34**:6219 (1986).
20. K. Sasaki and L. M. Floria, *J. Phys. Condensed Matter* **1**:2179 (1989).
21. K. E. Bassler, Ph.D. Dissertation, Carnegie-Mellon University, Pittsburgh, Pennsylvania (1990).
22. T. Nagamiya, in *Solid State Physics*, Vol. 20, F. Seitz, T. Turnbull, and H. Ehrenreich, eds. (Academic Press, New York, 1967), p. 305.
23. T. Nagamiya, K. Nagata, and Y. Kitano, *Prog. Theor. Phys.* **27**:1253 (1962).
24. Y. Kitano and T. Nagamiya, *Prog. Theor. Phys.* **31**:1 (1964).
25. R. B. Griffiths and W. Chou, *Phys. Rev. Lett.* **56**:1929 (1986).
26. J. Jensen and A. R. Mackintosh, *Phys. Rev. Lett.* **64**:2699 (1990).
27. L. M. Floría and R. B. Griffiths, *Numer. Math.* **55**:565 (1989).
28. R. B. Griffiths, in *Fundamental Problems in Statistical Mechanics VII*, H. van Beijeren, ed. (North-Holland, Amsterdam, 1990), p. 69.
29. L. H. Tang and R. B. Griffiths, *J. Stat. Phys.* **53**:853 (1988).
30. K. Sasaki, *Physica A* **171**:80 (1991).